Intertwined spin, charge, and pair correlations in the two-dimensional Hubbard model in the thermodynamic limit

Peizhi Mai[a], Seher Karakuzu[a], Giovanni Balduzzi[b], Steven Johnston[c], and Thomas A. Maier[a,1]

[a]Computational Sciences and Engineering Division, Oak Ridge National Laboratory, Oak Ridge, TN, 37831-6211; [b]Institute for Theoretical Physics, ETH Zurich, 8093 Zurich, Switzerland; and [c]Department of Physics and Astronomy, University of Tennessee, Knoxville, TN 37996-1200

Edited by Steven Kivelson, Department of Physics, Stanford University, Stanford, CA; received July 12, 2021; accepted November 17, 2021

The high-temperature superconducting cuprates are governed by intertwined spin, charge, and superconducting orders. While various state-of-the-art numerical methods have demonstrated that these phases also manifest themselves in doped Hubbard models, they differ on which is the actual ground state. Finite-cluster methods typically indicate that stripe order dominates, while embedded quantum-cluster methods, which access the thermodynamic limit by treating long-range correlations with a dynamical mean field, conclude that superconductivity does. Here, we report the observation of fluctuating spin and charge stripes in the doped single-band Hubbard model using a quantum Monte Carlo dynamical cluster approximation (DCA) method. By resolving both the fluctuating spin and charge orders using DCA, we demonstrate that they survive in the doped Hubbard model in the thermodynamic limit. This discovery also provides an opportunity to study the influence of fluctuating stripe correlations on the model's pairing correlations within a unified numerical framework. Using this approach, we also find evidence for pair-density-wave correlations whose strength is correlated with that of the stripes.

Hubbard model | stripe | dynamical cluster approximation

A common element of strongly correlated materials is the existence of several nearly degenerate states, which compete or cooperate to produce novel phases of matter (1). For example, in the high-temperature (high-T_c) superconducting cuprates, multiple theoretical studies and experiments point to intertwined orders of spin and charge stripes, charge-density waves, pair-density waves (PDWs), and unconventional superconductivity (1–7). Understanding the relationships among these orders and how they shape the cuprate phase diagram is a central problem in condensed-matter physics.

Addressing this question using nonpertubative methods remains challenging, as even the simplest correlated electron models also contain near-degenerate orders, which can be difficult to discern from one another. For example, state-of-the-art numerical studies have identified a plethora of low-energy states in the single-band Hubbard and t-J models that contend for the ground state (5, 6, 8–25). Methods like Hartree–Fock mean-field theory (10–12), density matrix renormalization group (5, 13–16), density matrix embedding theory (13, 17), variational Monte Carlo (18), auxiliary field quantum Monte Carlo (QMC) (5, 6, 13, 19), and infinite projected entangled-pair states (13, 20) tend to find static stripe order, i.e., unidirectional spin- and charge-density waves, as the ground state, and recent determinant QMC (DQMC) calculations (8, 9) and minimally entangled typical thermal states (25) have found evidence for spin-stripe correlations at finite temperatures. In contrast, quantum-cluster methods like cellular dynamical mean-field theory (24, 26, 27) and the dynamical cluster approximation (DCA) (28, 29), which, unlike finite size cluster techniques, directly access the thermodynamic limit, typically find superconducting solutions with a d-wave symmetry (21–24). While approximate calculations of this sort with large unit cells, but correlations restricted to single sites or small clusters, have found evidence of stripes (30–33), more reliable calculations with clusters large enough to accommodate the stripe periodicity have yet to find any indication of stripe-like solutions. It is crucial that we understand and resolve these differences to properly identify the properties of the Hubbard model in the thermodynamic limit. Moreover, this dichotomy has made it difficult to understand the relationships between the relevant orders since each method has its approximations, which introduce systematic errors that can bias toward particular solutions. To overcome this issue, it is desirable to identify a single framework capable of identifying the relevant states to avoid compounding systematic biases.

Here, we demonstrate that QMC DCA (28) methods can detect short-range stripe correlations in the two-dimensional, single-band Hubbard model. The QMC-based impurity solver captures the intracluster correlations exactly, while longer-range correlations are treated in a mean field that approximates the infinite system. The observation of fluctuating stripes with this method therefore provides crucial confirmation that such correlations persist in the thermodynamic limit. It also fixes the discrepancy between finite-cluster and quantum-cluster methods. Our results allow us to examine the influence of fluctuating stripe correlations on d-wave pairing in the single-band Hubbard model

Significance

The high-temperature superconducting cuprates are governed by intertwined striped magnetic and charge orders, in addition to superconductivity. Remarkably similar behavior has also been seen in numerical calculations for the Hubbard model describing the copper–oxygen layers in these materials. Finite-cluster methods typically find that spin- and charge-stripe order dominates, while embedded quantum-cluster methods, which access the thermodynamic limit, often conclude that superconductivity does. Here, we report the observation of fluctuating spin and charge stripes in an embedded cluster calculation for the Hubbard model. This discovery demonstrates that striped states survive in the thermodynamic limit and allows us to study their influence on the model's superconducting properties, where we find evidence for pair-density-wave correlations intertwined with the stripe correlations.

Author contributions: P.M. performed research; P.M., S.K., S.J., and T.A.M. analyzed data; P.M., S.J., and T.A.M. wrote the paper; and S.K. and G.B. developed code.

The authors declare no competing interest.

This article is a PNAS Direct Submission.

[1]To whom correspondence may be addressed. Email: maierta@ornl.gov.

This article contains supporting information online at https://www.pnas.org/lookup/suppl/doi:10.1073/pnas.2112806119/-/DCSupplemental.

Published February 9, 2022.

using a unified framework, provided the clusters are large enough to accommodate the relevant periodicity, such that the spatial modulations are not averaged out by the DCA mean field. Using this unified framework, we find evidence for short-range PDW correlations, whose strength is correlated with the strength of the spin- and charge-stripe correlations.

Model

We consider the two-dimensional, single-band Hubbard Hamiltonian defined on a rectangular $N = N_x \times N_y$ lattice

$$H = -\sum_{\mathbf{i},\mathbf{j},\sigma} t_{\mathbf{ij}} \left(c^{\dagger}_{\mathbf{i}\sigma} c_{\mathbf{j}\sigma} + \text{h.c.} \right) - \mu \sum_{\mathbf{i},\sigma} n_{\mathbf{i}\sigma} + U \sum_{\mathbf{i}} n_{\mathbf{i}\uparrow} n_{\mathbf{i}\downarrow}. \quad [1]$$

Here, $c^{\dagger}_{\mathbf{i}\sigma}$ ($c_{\mathbf{i}\sigma}$) creates (annihilates) a spin-σ ($=\uparrow,\downarrow$) electron on site $\mathbf{i}$; $n_{\mathbf{i}\sigma} = c^{\dagger}_{\mathbf{i},\sigma} c_{\mathbf{i}\sigma}$ is the number operator; $t_{\mathbf{ij}}$ is the hopping integral between sites $\mathbf{i}$ and $\mathbf{j}$; μ is the chemical potential; and U is the on-site Hubbard repulsion. Throughout, we restrict $t_{\mathbf{ij}}$ to nearest-neighbor (t) and next-nearest-neighbor (t') hopping only and set $U = 6t$ to facilitate comparisons to ref. 8. We then solved Eq. **1** using DCA (28) and with a continuous-time QMC impurity solver (23), as implemented in the DCA++ code (34), and complementary DQMC calculations (35, 36).

Previous DQMC calculations (8, 9) have demonstrated that the high-temperature spin-stripe correlations in the single-band and multiband Hubbard model are fluctuating in nature, where short-range spatial correlations appear over several unit cells and are fluctuating in time. In general, static ($\omega = 0$) correlation functions, which integrate over the imaginary time dynamics, are expected to be more sensitive to fluctuating short-range order (37) compared to the corresponding equal-time ($\tau = 0$) correlation functions (8). We have found that this is indeed the case for the spin, charge, and PDW-like correlations reported here (*SI Appendix*), supporting the interpretation that the observed stripe correlations are fluctuating in nature.

To study the fluctuating spin stripes, we measured the static staggered spin–spin correlation function $S^{\text{stag}}(\mathbf{r}, \omega = 0) = (-1)^{r_x + r_y} \frac{1}{N} \int_0^{\beta} \sum_{\mathbf{i}} \langle \hat{S}^z_{\mathbf{i}+\mathbf{r}}(\tau)\ \hat{S}^z_{\mathbf{i}}(0) \rangle d\tau$, where $\mathbf{r} = a(r_x, r_y)$ is the position of each atom on the square lattice with lattice constant a, and $\hat{S}^z_{\mathbf{i}} = \frac{1}{2}\left(c^{\dagger}_{\mathbf{i},\uparrow} c_{\mathbf{i},\uparrow} - c^{\dagger}_{\mathbf{i},\downarrow} c_{\mathbf{i},\downarrow} \right)$ is the z-component of the local spin operator at site $\mathbf{i}$. The fluctuating charge-stripe correlations are assessed by measuring the static density–density correlation function $N(\mathbf{r}, \omega = 0) = \frac{1}{N} \int_0^{\beta} \sum_{\mathbf{i}} \left(\langle n_{\mathbf{i}+\mathbf{r}}(\tau)\ n_{\mathbf{i}}(0) \rangle - \langle n_{\mathbf{i}+\mathbf{r}}(\tau) \rangle \langle n_{\mathbf{i}}(0) \rangle \right) d\tau$, where $n_{\mathbf{i}} = \sum_{\sigma} n_{\mathbf{i},\sigma}$ is the local density operator. The pairing tendencies are accessed by measuring the static pairing correlation function in the d-wave channel $P_d(\mathbf{r}, \omega = 0) = \frac{1}{N} \int_0^{\beta} \sum_{\mathbf{i}} \langle \Delta_{\mathbf{i}+\mathbf{r}}(\tau)\ \Delta^{\dagger}_{\mathbf{i}}(0) \rangle d\tau$, where $\Delta_{\mathbf{i}} = c_{\mathbf{i},\uparrow}(c_{\mathbf{i}+\hat{x},\downarrow} + c_{\mathbf{i}-\hat{x},\downarrow} - c_{\mathbf{i}+\hat{y},\downarrow} - c_{\mathbf{i}-\hat{y},\downarrow}) - c_{\mathbf{i},\downarrow}(c_{\mathbf{i}+\hat{x},\uparrow} + c_{\mathbf{i}-\hat{x},\uparrow} - c_{\mathbf{i}+\hat{y},\uparrow} - c_{\mathbf{i}-\hat{y},\uparrow})$ destroys a singlet pair of electrons with d-wave symmetry. We also determined the structure of the pairing interaction by explicitly solving the Bethe–Salpeter equation in the particle–particle singlet channel to obtain its leading eigenvalues and eigenvectors (22, 38). Due to the large cluster sizes and the self-consistency loop, our DCA calculations are significantly more expensive than the corresponding DQMC calculations. For this reason, we focus on an average density, $\langle n \rangle = 0.8$, where we have observed strong stripe correlations.

Results and Discussion

Fig. 1 plots $S^{\text{stag}}(\mathbf{r})$ for several values of the next-nearest-neighbor hopping t', where we see clear evidence for spin-stripe correlations in our DCA calculations (Fig. 1 *A*, *B*, and *D*–*F*). Here, we employ large 16×4 clusters embedded in the DCA self-consistent mean field, where we access temperatures as low as $T = 0.167t$ (inverse temperature $\beta = 6/t$). Since the staggered spin–spin correlation function imposes a sign flip on every other site, the positive blue regions in the middle of each panel represent short-range antiferromagnetic (AFM) correlations. In contrast, the negative red regions represent AFM regions, but with a π phase shift. As t'/t decreases from positive to negative, red negative regions form more prominently on both sides of the central blue region, signaling the formation and growth of AFM stripe fluctuations, similar to those observed in finite-size DQMC calculations (8, 9). In general, we find that the boundary between the red and blue regions mixes, suggesting

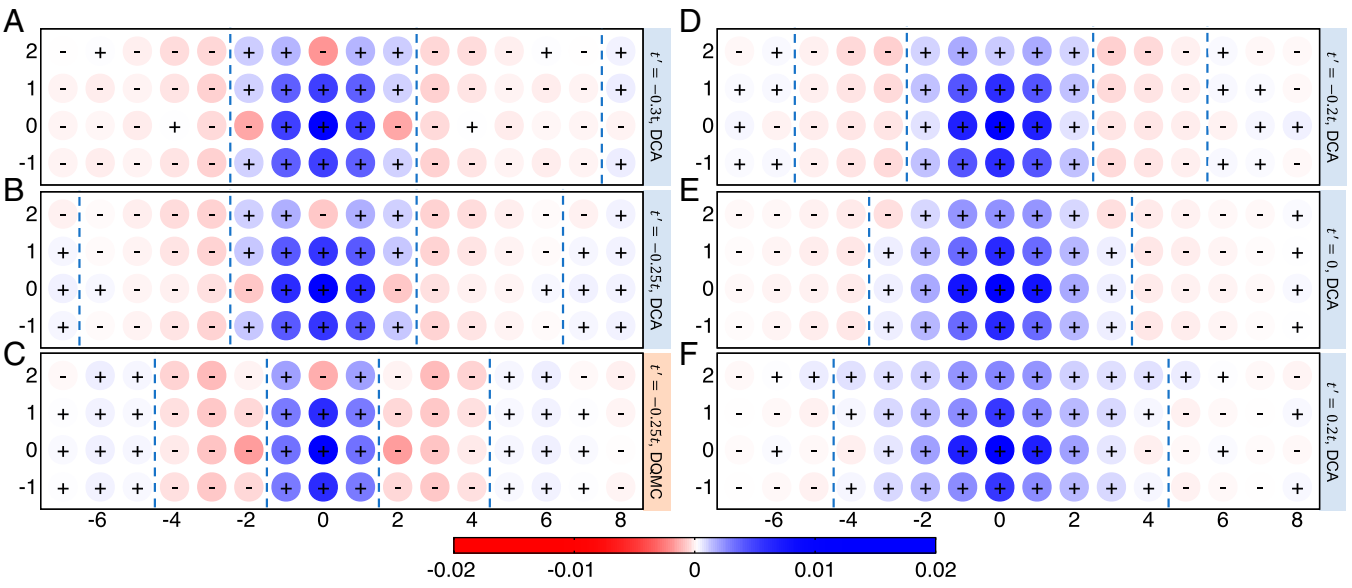

Fig. 1. The real-space static staggered spin–spin correlation function of the single-band Hubbard model with $\langle n \rangle = 0.8$, obtained from DCA and DQMC simulations. Results are shown for $t' = -0.3t$, DCA (*A*); $t' = -0.25t$, DCA (*B*); $t' = -0.25t$, DQMC (*C*); $t' = -0.2t$, DCA (*D*); $t' = 0$, DCA (*E*); and $t' = 0.2t$, DCA (*F*). The DCA results were obtained by using a 16×4 cluster embedded in a dynamical mean field and at an inverse temperature $\beta = 6/t$ (*A*, *B*, and *D*–*F*). The DQMC results shown in *C* were obtained on a 16×4 cluster with periodic boundary conditions and $\beta = 4.5/t$ and $t' = -0.25t$. Note that here and throughout, we have adopted the same custom color bars used in refs. 8 and 9. This scale provides a finer gradation of small values of the correlation function and improves the overall contrast (*SI Appendix*).

that the stripes are incommensurate. We have observed similar patterns for different cluster sizes and geometries, including 8×8, 8×6 and 8×4 clusters, and in the spin xx correlations (*SI Appendix*).

For comparison, Fig. 1*C* shows $S^{\mathrm{stag}}(\mathbf{r}, \omega = 0)$ obtained from a DQMC calculation at $T = 0.22t$ ($\beta = 4.5/t$), $t' = -0.25t$. The DQMC results are consistent with the corresponding DCA results (Fig. 1*B*). [A systematic comparison between DCA and an earlier DQMC study (8) focusing on the real-space equal-time spin–spin correlation function at the density $n = 0.875$ is given in *SI Appendix*.] Since DQMC treats the system exactly on an extended, but finite, cluster, one must perform a finite-size scaling analysis to access the thermodynamic limit. On the other hand, DCA accesses the thermodynamic limit by embedding its clusters in a dynamical mean field that approximates the rest of the system. Comparing Fig. 1 *B* and *C*, we find that DCA predicts weaker stripe correlations compared to DQMC for the same t', despite the lower temperature. This observation may help explain why stripes have previously gone unobserved in quantum-cluster approaches employing extended clusters. The origin of the reduced correlations is unclear at this time. One possibility is that the correlations observed by DQMC would weaken as the cluster size increases. Another is that the mean field reduces the effective correlations in the DCA treatment of the problem or tends to favor uniform states and restore C_4 symmetry in the cluster. Nevertheless, the observation of stripes with DCA provides crucial evidence that they persist in the thermodynamic limit.

Although we observe similar fluctuating spin stripes in both zero-frequency (Fig. 1) and equal-time (*SI Appendix*) spin–spin correlation functions, the zero-frequency (Fig. 2) and equal-time (*SI Appendix*) density–density correlation functions show qualitatively different behaviors. The density–density correlations have much stronger imaginary time dependence. A detailed imaginary time analysis can be found in *SI Appendix*. As a result, the fluctuating charge-stripe pattern is only observed in the static ($\omega = 0$) correlation functions. Fig. 2 plots $N(\mathbf{r}, \omega = 0)$ for the same 16×4 DCA and DQMC simulations shown in Fig. 1. We observe the central blue region surrounded by two red regions on both sides, signaling short-range charge-stripe fluctuations, but with a shorter period. As t'/t increases from negative to positive, unlike the spin case, where the blue region extends to weaken the stripe, the charge blue region does not extend. In the electron-doped case ($t' = 0.2t$), however, the central region is dominated by a staggered (π, π) CDW-like correlation, with the subdominant stripe-like pattern laying on both sides. As a comparison, the DQMC result in Fig. 2*C* shows a stronger stripe pattern with a shorter period than the corresponding DCA result in Fig. 2*B*.

The presence of the spin and charge stripes is more readily observed by examining the dynamical spin $S(\mathbf{Q}, \omega)$ and charge $N(\mathbf{Q}, \omega)$ susceptibilities (37), which measure the collective fluctuations. Here, we consider the static limit ($\omega = 0$), which can be obtained by Fourier transforming the corresponding static real-space correlation functions. Fig. 3 summarizes $S(\mathbf{Q}, \omega = 0)$ along $\mathbf{Q} = (Q_x, \pi)$ (Fig. 3 *A*–*E*) and $N(\mathbf{Q}, \omega = 0)$ along $\mathbf{Q} = (Q_x, 0)$ (Fig. 3 *F*–*J*) for different values of the next-nearest-neighbor hopping t'. When the spin-stripe correlations are strong, they should manifest as incommensurate peaks in $S(\mathbf{Q}, 0)$ centered at $(2\pi/a)(0.5 \pm \delta_s, 0.5)$, while the charge stripes should manifest as incommensurate peaks in $N(\mathbf{Q}, 0)$ centered at $(2\pi/a)(\pm\delta_c, 0)$, where $\delta_c = 2\delta_s$. To check this, we fit the spectra with pairs of Lorentzian functions (plus a constant background) and extracted the corresponding values of $\delta_{s,c}$. In all cases, the susceptibilities are well represented by the fits, and the resulting ratio $r = \delta_s/\delta_c$ is given in Fig. 3 *A*–*E*, where we find $0.66 > r > 0.3$. Especially in the cases with $t' < 0$, these values are close to the expected $r = 0.5$ result, for which the periodicity of the charge fluctuations is twice that of the spin fluctuations.

To examine how the spin and charge stripes form, we also extracted the values of δ_c, δ_s, and $r = \delta_s/\delta_c$ as a function of temperature for $t' = -0.3t$, as shown in Fig. 3*K*. (The corresponding susceptibility data are provided in *SI Appendix*.) We find that δ_s remains relatively fixed as a function of temperature, while δ_c appears to lock in to its value of $\delta_c \approx 2\delta_s$ as the temperature is lowered. From Figs. 1–3, we can see that the incommensurability δ_s (or period) of the fluctuating spin stripes depends weakly on temperature but strongly on t', while the incommensurability δ_c (or period) of the fluctuating charge stripes depends strongly on temperature, but weakly on t'. Fig. 3 *L* and *M* show the correlation lengths ξ_s and ξ_c for $t' = -0.3t$ for the fluctuating spin and charge stripes, respectively. These values are determined from the inverse of the half-width-half-maximum of the Lorentzian

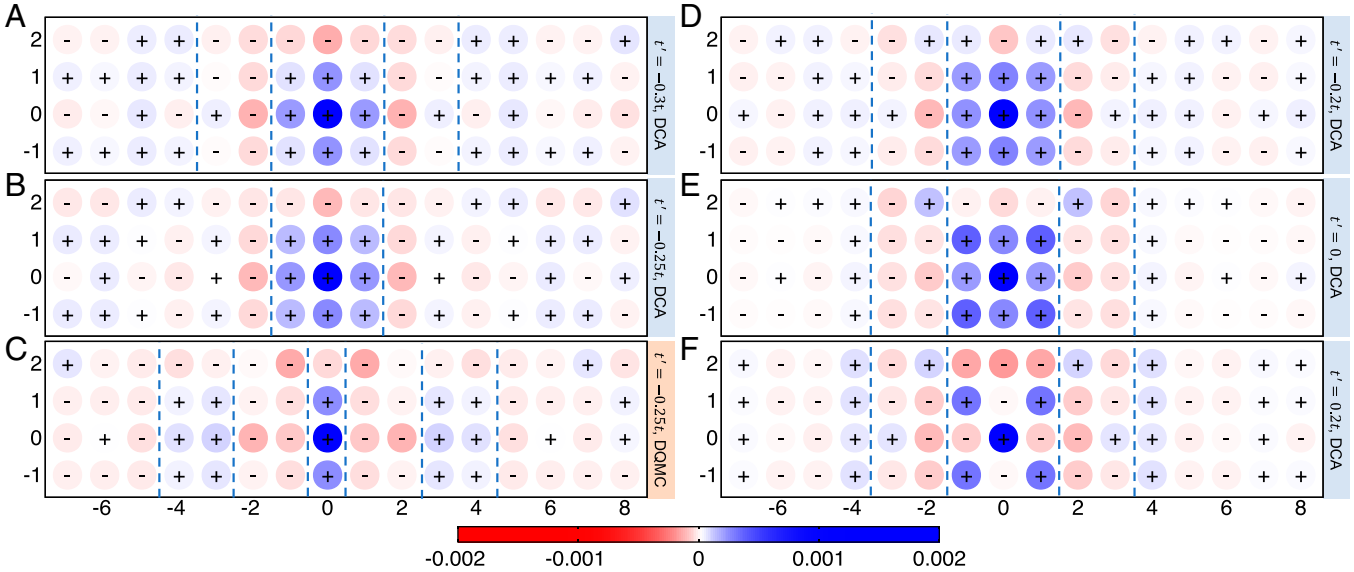

Fig. 2. The real-space static density-density correlation function of the single-band Hubbard model, obtained from DCA and DQMC simulations. Results are shown for $t' = -0.3t$, DCA (A); $t' = -0.25t$, DCA (B); $t' = -0.25t$, DQMC (C); $t' = -0.2t$, DCA (D); $t' = 0$, DCA (E); and $t' = 0.2t$, DCA (F). The DCA results were obtained by using a 16×4 cluster embedded in a dynamical mean field and at an inverse temperature $\beta = 6/t$ (A, B, and D–F). The DQMC results shown in C were obtained on a 16×4 cluster with periodic boundary conditions and $\beta = 4.5/t$ and $t' = -0.25t$.

https://doi.org/10.1073/pnas.2112806119

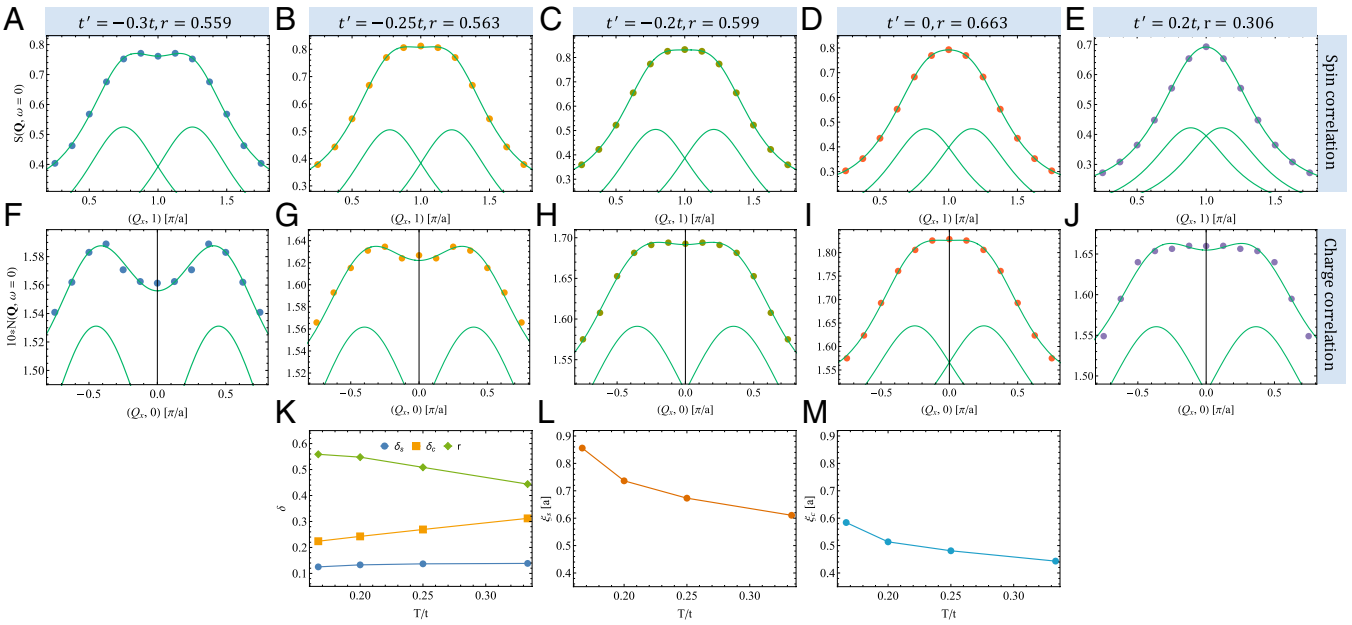

Fig. 3. DCA results for the static spin $S(\mathbf{Q}, \omega = 0)$ (*A–E*) and charge $N(\mathbf{Q}, \omega = 0)$ (*F–J*) susceptibilities, obtained on a 16 × 4 cluster embedded in a dynamical mean field and with $\langle n \rangle = 0.8$. *A–E* show the spin susceptibilities along $\mathbf{Q} = (Q_x, \pi)$ for $t' = -0.3t$ (*A*), $t' = -0.25t$ (*B*), $t' = -0.2t$ (*C*), $t' = 0$ (*D*), and $t' = 0.2t$ (*E*). Each curve is fit with a pair of Lorentzian functions centered at $(2\pi/a)(0.5 \pm \delta_s, 0.5)$ plus a constant background. *F–J* show the corresponding charge susceptibilities along $\mathbf{Q} = (Q_x, 0)$. Each curve is fit with a pair of Lorentzian functions centered at $(2\pi/a)(\pm\delta_c, 0)$ plus a constant background. All results were obtained for $T = 0.167t$ ($\beta = 6/t$). The ratio of the spin and charge incommensurabilities is given by $r = \delta_s/\delta_c$, and *K* shows the temperature evolution of the spin and charge incommensurabilities and their ratio *r* for $t' = -0.3t$. *L* and *M* show the temperature dependence of the spin and charge correlation lengths, respectively, for the same t'.

fits, but we obtain very similar estimates from exponential fits of the real-space correlations. We find that both the spin- and charge-correlation lengths extracted this way are relatively short at the temperatures we can access, but grow with decreasing temperature. We also find that the charge correlation length is substantially shorter than the spin correlation length. These results suggest that in the hole-doped case, the charge stripes emerge at lower energy scales than spin stripes do in the Hubbard model and that the periodicity of the former locks into the value set by the latter. This finding is counter to the idea that the charge order forms prior to the spin order (39, 40). In the electron-doped case, the comparison between Figs. 1*F* and 2*F* shows that the charge stripe appears at higher energy scale instead.

Previous DCA studies have observed a finite-temperature transition to the *d*-wave superconducting state (21, 38). Now that DCA also finds evidence for fluctuating stripes, both in the spin and charge sector, it is natural to ask how they affect the formation of Cooper pairs. To answer this question, we examine the static *d*-wave pairfield susceptibility $P_d(\mathbf{r}, \omega = 0)$ calculated with DCA on a 16 × 4 cluster, as shown in Fig. 4. Interestingly, as t' is reduced and varied to more negative values, the static pairfield correlations develop a modulated striped pattern with a sign change (π phase shift) suggestive of a PDW (3). This trend is similar to that found for the spin-stripe fluctuations in Fig. 1, except that for $t' = -0.25t$, the modulation is less visible, possibly due to a change in the Fermi surface topology from electron- to hole-like (41). Fig. 5 shows the corresponding plots of the Fourier-transformed static *d*-wave pairfield susceptibility $P_d(\mathbf{Q}, \omega = 0)$ fitted with a pair of Lorentzian functions. For $t' = 0.2t$, we observe a single peak at $\mathbf{Q} = (0, 0)$. But as t' is lowered and varied to more negative values, one sees that the peak flattens out. In this case, the best fit is obtained with two separate Lorentzians centered at $(2\pi/a)(\pm\delta_P, 0)$, consistent with the periodic PDW-like modulation observed in Fig. 4.

These observations suggest that striped modulations in the pairfield correlations develop together with the spin- and charge-stripe correlations. At the temperatures we have studied,

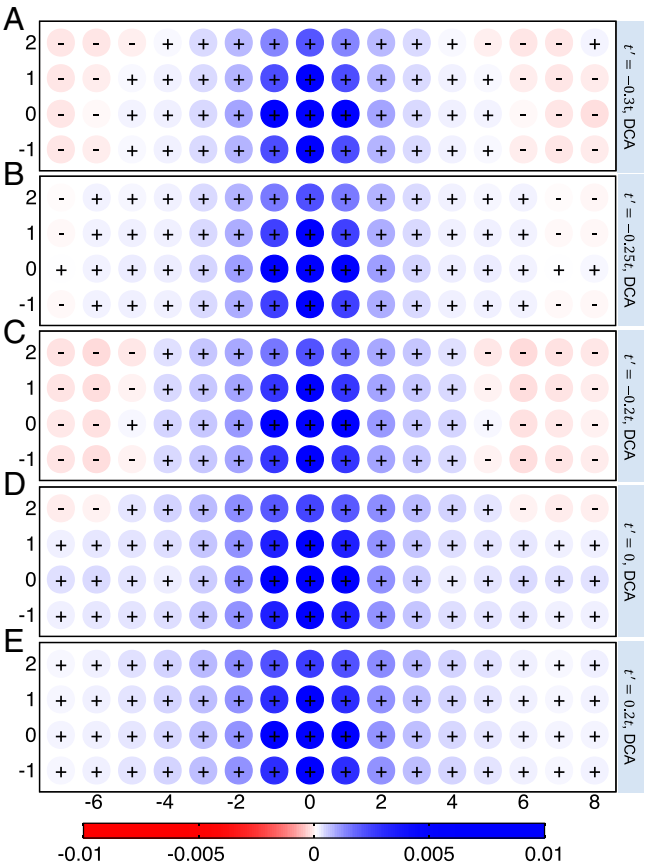

Fig. 4. The real-space static *d*-wave pairfield correlation function of the single-band Hubbard model. DCA results are shown for $t' = -0.3t$ (A), $-0.25t$ (B), $-0.2t$ (C), 0 (D), and $0.2t$ (E). The remaining model parameters are identical to those used in Fig. 1.

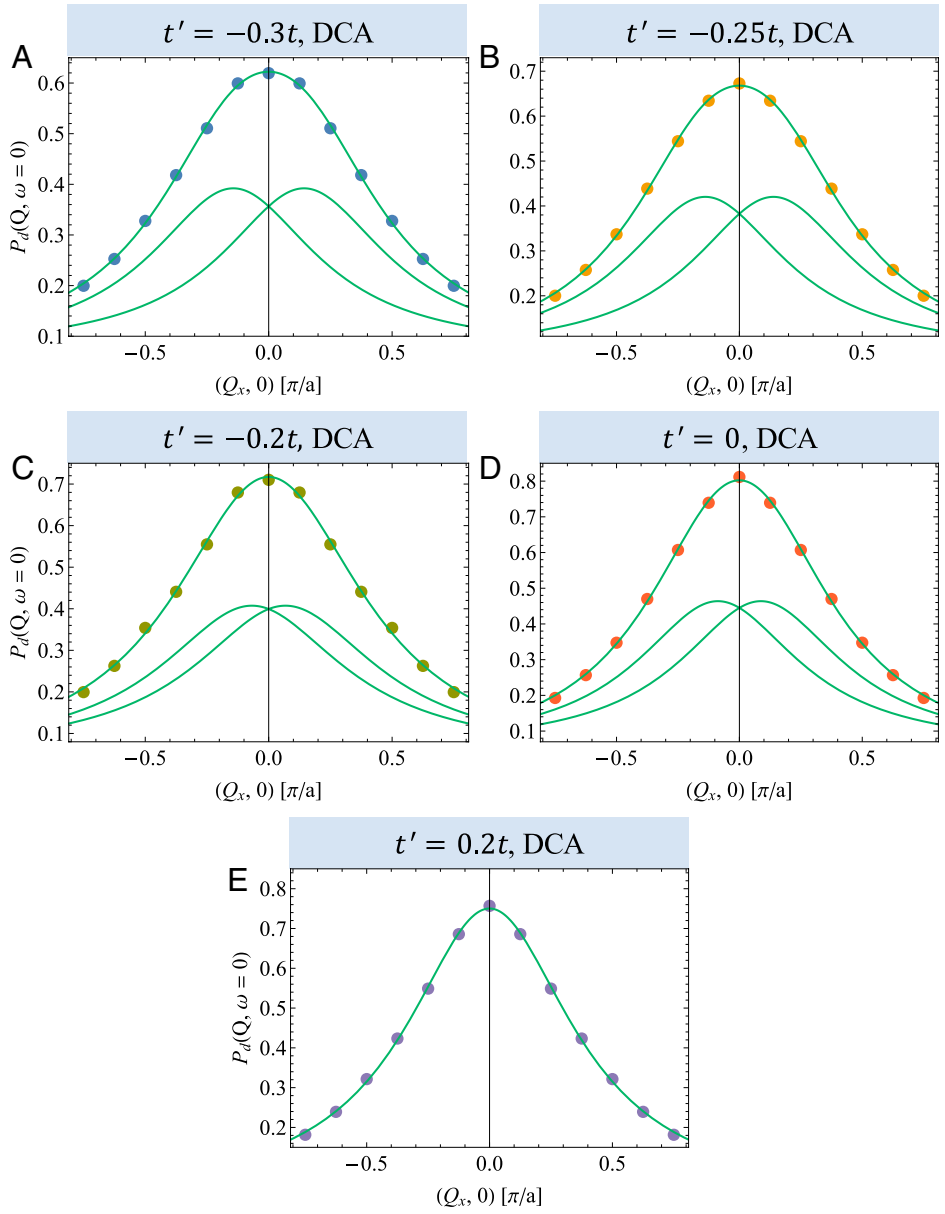

Fig. 5. DCA results for the static pairfield susceptibility $P_d(\mathbf{Q}, \omega = 0)$ for $\langle n \rangle = 0.8$ and $T = 0.167t$ ($\beta = 6/t$) obtained on a 16×4 cluster embedded in a dynamical mean field for $t' = -0.3t$ (*A*), $t' = -0.25t$ (*B*), $t' = -0.2t$ (*C*), $t' = 0$ (*D*), and $t' = 0.2t$ (*E*). Each curve is fit with a pair of Lorentzian functions centered at $(\pm\delta_P, 0)$. For $t' = 0.2t$, the two Lorentzians collapse onto a single peak centered at $(0, 0)$.

it is clear from Fig. 5 that their signature in the momentum structure of the pairfield susceptibility is not as strong as that of the spin and charge stripes. Nevertheless, the striped modulation is clearly visible in the real space structure in Fig. 4. Whether the PDW-like modulations become stronger at lower temperatures and potentially lead to a superconducting instability to a PDW state, however, remains an open question that we are unable to address because of the Fermion sign problem.

Conclusion

Our results demonstrate that fluctuating spin- and charge-stripe orders are a property of the doped single-band Hubbard model in the thermodynamic limit. Moreover, by accessing these phases using an embedded cluster technique, we are able to examine the ways in which the stripe fluctuations couple to superconducting correlations in the model. Concomitant with the spin stripes, we find that the *d*-wave pairing correlations develop a similar periodic stripe modulation, indicative of a pair-density wave.

Materials and Methods

DCA. To study the single-band Hubbard model, we use the DCA (21, 28, 29, 34). Complete details of the DCA algorithm can be found in ref. 29. The DCA coarse-grains momentum space to represent the bulk lattice in the thermodynamic limit by a finite size cluster that contains N_c sites and is embedded in a self-consistent mean field. This mean field represents the remaining degrees of freedom and is determined self-consistently from the solution of the cluster problem.

With the assumption of short-ranged correlations, the self-energy $\Sigma(\mathbf{k}, i\omega_n)$ is well approximated by the cluster self-energy $\Sigma(\mathbf{K}, i\omega_n)$, where $\mathbf{K}$ are the cluster momenta. The coarse-grained, single-particle Green's function

$$\bar{G}(\mathbf{K}, i\omega_n) = \frac{N_c}{N} \sum_{\mathbf{k}'} G(\mathbf{K} + \mathbf{k}', i\omega_n) = \frac{N_c}{N} \sum_{\mathbf{k}'} \frac{1}{i\omega_n + \mu - \varepsilon(\mathbf{K} + \mathbf{k}') - \Sigma(\mathbf{K}, i\omega_n)}, \quad [2]$$

is then obtained by averaging the lattice Green's function $G(\mathbf{k}, i\omega_n)$ over the N/N_c momenta $\mathbf{k}'$ in a square patch about the cluster momentum $\mathbf{K}$ that has

an area of size $1/N_c$ of that of the first Brillouin zone. This reduces the bulk problem to a finite size cluster, which we solve using the continuous-time, auxiliary-field, QMC algorithm (CT-AUX) (23).

In our DCA++ simulations, the expansion order of the CT-AUX QMC is typically in the range of 100 to 3,000, depending on temperature and t'. Depending on the average fermion sign for a given parameter set, we have obtained 10 million to 2 billion samples for the correlation functions. Usually, six to eight iterations were needed to obtain good convergence for the DCA mean field.

DQMC. We also perform DQMC (35, 36) simulation on the single-band Hubbard model to obtain the spin, charge, and pairing correlation functions for finite-size clusters. We divide the imaginary time interval $[0, \beta]$ into L discrete steps with step size fixed at $\Delta\tau = 0.1$ and rewrite the partition function using the Trotter formula neglecting terms of order $\mathcal{O}(\Delta\tau^2)$.

We perform equal-time measurements every other full space-time sweep and unequal-time measurements every fourth sweep. We use 5,000 independently seeded Markov chains, and, for each chain, we use 50,000 warmup sweeps and 400,000 measurement sweeps. This large amount of data leads to reliable statistics, despite the severe Fermion sign problem.

Data Availability. The entire dataset has been deposited on Zenodo, https://doi.org/10.5281/zenodo.5904352 (42).

ACKNOWLEDGMENTS. We thank T. P. Devereaux, E. Huang, B. Moritz, and D. J. Scalapino for useful discussions. This work was supported by the Scientific Discovery through Advanced Computing program funded by the US Department of Energy (DOE), Office of Science, Advanced Scientific Computing Research and Basic Energy Sciences, Division of Materials Sciences and Engineering. This research used resources of the Oak Ridge Leadership Computing Facility, which is a DOE Office of Science User Facility supported under Contract DE-AC05-00OR22725. A part of the analysis of the results performed by T.A.M. was supported by the DOE, Office of Basic Energy Sciences, Materials Sciences and Engineering Division. This manuscript has been authored by UT-Battelle, LLC, under Contract DE-AC05-00OR22725 with the DOE. The US Government retains and the publisher, by accepting the article for publication, acknowledges that the US Government retains a nonexclusive, paid-up, irrevocable, worldwide license to publish or reproduce the published form of this manuscript, or allow others to do so, for US Government purposes. The DOE will provide public access to these results of federally sponsored research in accordance with the DOE Public Access Plan (http://www.energy.gov/downloads/doe-public- access-plan).

1. E. Fradkin, S. A. Kivelson, J. M. Tranquada, Colloquium: Theory of intertwined orders in high temperature superconductors. *Rev. Mod. Phys.* **87**, 457–482 (2015).
2. J. M. Tranquada, B. J. Sternlieb, J. D. Axe, Y. Nakamura, S. Uchida, Evidence for stripe correlations of spins and holes in copper oxide superconductors. *Nature* **375**, 561–563 (1995).
3. D. F. Agterberg *et al.*, The physics of pair-density waves: Cuprate superconductors and beyond. *Annu. Rev. Condens. Matter Phys.* **11**, 231–270 (2020).
4. J. M. Tranquada, Cuprate superconductors as viewed through a striped lens. *Adv. Phys.* **69**, 437–509 (2021).
5. M. Qin *et al.*, Absence of superconductivity in the pure two-dimensional Hubbard model. *Phys. Rev. X* **10**, 031016 (2020).
6. M. Qin, T. Schäfer, S. Andergassen, P. Corboz, E. Gull, The Hubbard model: A computational perspective. arXiv [Preprint] (2021). https://arxiv.org/abs/2104.00064 (Accessed 31 March 2021).
7. R. Arpaia, G. Ghiringhelli, Charge order at high temperature in cuprate superconductors. *J. Phys. Soc. Jpn.* **90**, 111005 (2021).
8. E. W. Huang, C. B. Mendl, H. C. Jiang, B. Moritz, T. P. Devereaux, Stripe order from the perspective of the Hubbard model. *NPJ Quantum Mater.* **3**, 22 (2018).
9. E. W. Huang *et al.*, Numerical evidence of fluctuating stripes in the normal state of high-T_c cuprate superconductors. *Science* **358**, 1161–1164 (2017).
10. J. Zaanen, O. Gunnarsson, Charged magnetic domain lines and the magnetism of high-Tc oxides. *Phys. Rev. B Condens. Matter* **40**, 7391–7394 (1989).
11. K. Machida, Magnetism in La_2CuO_4 based compounds. *Physica C* **158**, 192–196 (1989).
12. M. Kato, K. Machida, H. Nakanishi, M. Fujita, Soliton lattice modulation of incommensurate spin density wave in two dimensional Hubbard model—A mean field study. *J. Phys. Soc. Jpn.* **59**, 1047–1058 (1990).
13. B. X. Zheng *et al.*, Stripe order in the underdoped region of the two-dimensional Hubbard model. *Science* **358**, 1155–1160 (2017).
14. S. R. White, D. J. Scalapino, Stripes on a 6-leg Hubbard ladder. *Phys. Rev. Lett.* **91**, 136403 (2003).
15. H. C. Jiang, T. P. Devereaux, Superconductivity in the doped Hubbard model and its interplay with next-nearest hopping t'. *Science* **365**, 1424–1428 (2019).
16. Y. F. Jiang, J. Zaanen, T. P. Devereaux, H. C. Jiang, Ground state phase diagram of the doped Hubbard model on the four-leg cylinder. *Phys. Rev. Res.* **2**, 033073 (2020).
17. B. X. Zheng, G. K. L. Chan, Ground-state phase diagram of the square lattice Hubbard model from density matrix embedding theory. *Phys. Rev. B* **93**, 035126 (2016).
18. K. Ido, T. Ohgoe, M. Imada, Competition among various charge-inhomogeneous states and *d*-wave superconducting state in Hubbard models on square lattices. *Phys. Rev. B* **97**, 045138 (2018).
19. S. Sorella, The phase diagram of the Hubbard model by variational auxiliary field quantum Monte Carlo. arXiv [Preprint] (2021). https://arxiv.org/abs/2101.07045 (Accessed 18 January 2021).
20. P. Corboz, T. M. Rice, M. Troyer, Competing states in the *t-J* model: Uniform *D*-wave state versus stripe state. *Phys. Rev. Lett.* **113**, 046402 (2014).
21. T. A. Maier, M. Jarrell, T. C. Schulthess, P. R. C. Kent, J. B. White, Systematic study of *d*-wave superconductivity in the 2D repulsive Hubbard model. *Phys. Rev. Lett.* **95**, 237001 (2005).
22. T. A. Maier, M. S. Jarrell, D. J. Scalapino, Structure of the pairing interaction in the two-dimensional Hubbard model. *Phys. Rev. Lett.* **96**, 047005 (2006).
23. E. Gull, P. Werner, O. Parcollet, M. Troyer, Continuous-time auxiliary-field Monte Carlo for quantum impurity models. *Eur. Lett.* **82**, 57003 (2008).
24. G. Sordi, P. Sémon, K. Haule, A. M. S. Tremblay, Strong coupling superconductivity, pseudogap, and Mott transition. *Phys. Rev. Lett.* **108**, 216401 (2012).
25. A. Wietek, Y. Y. He, S. R. White, A. Georges, E. M. Stoudenmire, Stripes, antiferromagnetism, and the pseudogap in the doped Hubbard model at finite temperature. *Phys. Rev. X* **11**, 031007 (2021).
26. A. Foley, S. Verret, A. M. S. Tremblay, D. Sénéchal, Coexistence of superconductivity and antiferromagnetism in the Hubbard model for cuprates. *Phys. Rev. B* **99**, 184510 (2019).
27. G. Kotliar, S. Savrasov, G. Pálsson, G. Biroli, Cellular dynamical mean field approach to strongly correlated systems. *Phys. Rev. Lett.* **87**, 186401 (2001).
28. M. Jarrell, T. Maier, C. Huscroft, S. Moukouri, Quantum Monte Carlo algorithm for nonlocal corrections to the dynamical mean-field approximation. *Phys. Rev. B Condens. Matter Mater. Phys.* **64**, 195130 (2001).
29. T. Maier, M. Jarrell, T. Pruschke, M. H. Hettler, Quantum cluster theories. *Rev. Mod. Phys.* **77**, 1027–1080 (2005).
30. R. Peters, N. Kawakami, Spin density waves in the Hubbard model: A DMFT approach. *Phys. Rev. B Condens. Matter Mater. Phys.* **89**, 155134 (2014).
31. M. Fleck, A. Lichtenstein, E. Pavarini, One-dimensional metallic behavior of the stripe phase in $La_{2-x}Sr_xCuO_4$. *Phys. Rev. Lett.* **84**, 4962–4965 (2000).
32. T. I. Vanhala, P. Törmä, Dynamical mean-field theory study of stripe order and d-wave superconductivity in the two-dimensional Hubbard model. *Phys. Rev. B* **97**, 075112 (2018).
33. S. S. Dash, D. Sénéchal, Charge- and pair-density-wave orders in the one-band Hubbard model from dynamical mean field theory. *Phys. Rev. B* **103**, 045142 (2021).
34. U. R. Hähner *et al.*, DCA++: A software framework to solve correlated electron problems with modern quantum cluster methods. *Comput. Phys. Commun.* **246**, 106709 (2020).
35. R. Blankenbecler, D. J. Scalapino, R. L. Sugar, Monte Carlo calculations of coupled boson-fermion systems. I. *Phys. Rev. D Part. Fields* **24**, 2278–2286 (1981).
36. S. R. White *et al.*, Numerical study of the two-dimensional Hubbard model. *Phys. Rev. B Condens. Matter* **40**, 506–516 (1989).
37. S. A. Kivelson *et al.*, How to detect fluctuating stripes in the high-temperature superconductors. *Rev. Mod. Phys.* **75**, 1201–1241 (2003).
38. P. Mai, G. Balduzzi, S. Johnston, T. Maier, Orbital structure of the effective pairing interaction in the high-temperature superconducting cuprates. *NPJ Quantum Mater.* **6**, 26 (2021).
39. O. Zachar, S. A. Kivelson, V. J. Emery, Landau theory of stripe phases in cuprates and nickelates. *Phys. Rev. B Condens. Matter Mater. Phys.* **57**, 1442 (1998).
40. E. Berg *et al.*, Dynamical layer decoupling in a stripe-ordered high-T_c superconductor. *Phys. Rev. Lett.* **99**, 127003 (2007).
41. W. Wu *et al.*, Pseudogap and Fermi-surface topology in the two-dimensional Hubbard model. *Phys. Rev. X* **8**, 21048 (2018).
42. P. Mai, S. Karakuzu, G. Balduzzi, S. Johnston, T. A. Maier, Data set for "Intertwined spin, charge, and pair correlations in the two-dimensional Hubbard model in the thermodynamic limit." Zenodo. https://doi.org/10.5281/zenodo.5904352. Deposited 26 January 2022.